Inorganic Chemistry

Article

pubs.acs.org/IC

Facile Formation of Mesoporous $BiVO_4$/Ag/AgCl Heterostructured Microspheres with Enhanced Visible-Light Photoactivity

Ru Qiao,[†] Mengmeng Mao,[†] Enlai Hu,[†] Yijun Zhong,*[,†] Jiqiang Ning,*[,‡] and Yong Hu*[,†]

[†]Key Laboratory of the Ministry of Education for Advanced Catalysis Materials, Institute of Physical Chemistry, Zhejiang Normal University, Jinhua 321004, P. R. China

[‡]Vacuum Interconnected Nanotech Workstation, Suzhou Institute of Nano-Tech and Nano-Bionics, Chinese Academy of Sciences, Suzhou 215123, P. R. China

Supporting Information

ABSTRACT: In this study, we demonstrate a facile and novel dual-ion-exchange method together with subsequent visible-light induced reduction for synthesis of mesoporous $BiVO_4$/Ag/AgCl ternary heterostructured microspheres (HSMSs) with uniform size distribution. Using flower-like BiOCl microspheres as the starting material, and introducing $NaVO_3$ and $AgNO_3$ by a facile impregnation method, mesoporous $BiVO_4$/AgCl HSMSs have been obtained through solid-phase dual-ion-exchange reactions at 400 °C for 2 h. Interestingly, it has been found that Ag^+ ions play an indispensable role on the dual-ion-exchange reactions, and then the $BiVO_4$/AgCl HSMSs are converted into $BiVO_4$/Ag/AgCl ternary HSMSs by a facile visible-light illumination for 2 h. The as-prepared mesoporous $BiVO_4$/Ag/AgCl ternary HSMSs manifest high photocatalytic activity in degrading methyl orange (MO) and phenol under visible-light illumination, and a possible Z-scheme photocatalytic mechanism is proposed to understand the enhanced photochemical properties.

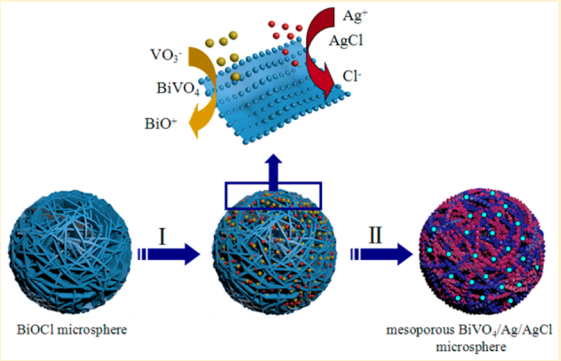

1. INTRODUCTION

Semiconductor heterostructures often have unique and/or enhanced physical and chemical properties compared to their respective counterparts, and hence have been extensively explored for their promising applications such as in electronic storage devices and photocatalysts.[1−3] For example, semiconductor heteronanostructures can not only prominently increase light-harvesting efficiency but also promote charge separation and transfer effectively, leading to improved photocatalytic activity.[4−11] Porous nanostructures of hybrid materials with uniform morphology and good structural stability have also attracted considerable interest owing to their high specific surface area and widespread applications in many different fields.[12−14] However, despite some successful preparation of porous heteronanostructures,[15,16] tailored synthesis of porous heterostructures toward practical photocatalytic applications is still very limited, especially due to the structural incompatibility between hybrid materials. It is therefore a great challenge to develop facile and reliable strategies to produce porous heterostructured semiconductor materials.[17,18]

With unique optical properties and hierarchical structures, bismuth compounds and their composites have attracted tremendous attention for their heterogeneous photocatalysis applications.[19−21] As an example, monoclinic scheelite bismuth vanadate (*m*-$BiVO_4$), with a narrow band gap of 2.4 eV, is an important visible-light responsive photocatalyst, which has been widely used in photodegradation of organic contaminants and photocatalytic evolution of O_2.[22−24] However, due to the rapid recombination of photogenerated electrons and holes, it has been found that the photocatalytic activity of $BiVO_4$ is usually not satisfactory in practical applications.[25] As one solution to this problem, combining two or more semiconductors with appropriate band alignment can considerably improve electron−hole pair separation and interfacial charge transfer efficiency, leading to effective promotion of photocatalytic activity.[26,27] $BiVO_4$/Cu_2O and $BiVO_4$/CeO_2 nanocomposites are some representative examples reported to exhibit much enhanced photocatalytic activity.[28,29]

In this study, we demonstrate a facile and novel method for controlled fabrication of mesoporous $BiVO_4$/Ag/AgCl ternary heterostructured microspheres (HSMSs) via a solid-phase dual-ion-exchange strategy together with subsequent visible-light induced reduction by using uniform BiOCl microspheres as the starting material. The synthesis strategy is schematically illustrated in Figure 1. As the precursor in this synthesis, uniform flower-like BiOCl microspheres, assembled from nanoflakes, are obtained via a simple solvothermal method. At stage I, $NaVO_3$ and $AgNO_3$ are first introduced into the BiOCl microspheres at room temperature through a facile impregnation method, which provides homogeneous distribu-

Received: June 10, 2015
Published: September 10, 2015

DOI: 10.1021/acs.inorgchem.5b01303
Inorg. Chem. 2015, 54, 9033−9039

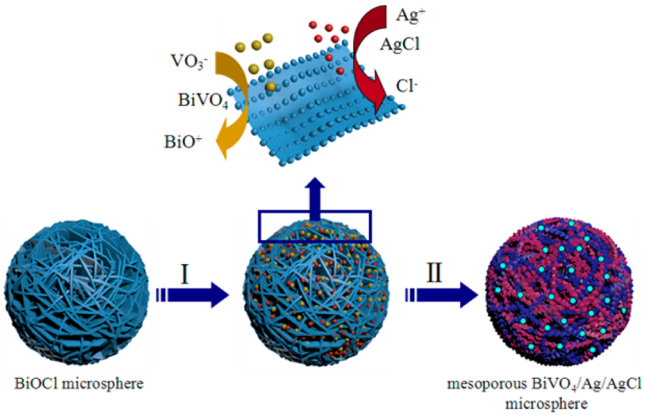

Figure 1. Schematic illustration of the formation of mesoporous $BiVO_4$/Ag/AgCl ternary HSMSs via a solid-phase dual-ion-exchange reaction method together with subsequent visible-light induced reduction process.

tion of the reagents at the nanoscale.[30] The solid-state dual-ion-exchange reactions take place during the 2-h annealing process at 400 °C, through which BiOCl microspheres are fully converted into mesoporous $BiVO_4$/AgCl binary HSMSs. The involved chemical reactions for the preparation of $BiVO_4$/AgCl HSMSs can be described as follows:

$$Ag^+ + Cl^- \rightarrow AgCl \quad (1)$$

$$BiOCl + VO_3^- \rightarrow BiVO_4 + Cl^- \quad (2)$$

The two reactions take place simultaneously through a solid-phase ion-exchange process which is hard to achieve at a low temperature in solution. Very interestingly, it has been found that Ag^+ ions play an indispensable role on the dual-ion-exchange reactions. In step II, ternary products of $BiVO_4$/Ag/AgCl ternary HSMSs are fabricated from the $BiVO_4$/AgCl binary HSMSs through a simple visible-light induced reduction process for 2 h. As expected, the as-prepared mesoporous $BiVO_4$/Ag/AgCl ternary HSMSs manifest high photocatalytic activity in degrading methyl orange (MO) and colorless organic phenol under visible-light illumination. In addition, a possible Z-scheme photocatalytic mechanism is proposed to understand the enhanced photochemical properties.

2. EXPERIMENTAL SECTION

All reagents were of analytical grade, purchased from the Shanghai Chemical Reagent Factory and used as received without further purification.

Synthesis of BiOCl Microspheres. In a typical synthesis, 0.12 g of $Bi(NO_3)_3{\cdot}5H_2O$, 0.03 g of NaCl, and 0.5 g of polyvinylpyrrolidone (PVP, MW ~ 58K) were dissolved in 35 mL of ethylene glycol (EG), and were well-dispersed with the assistance of sonication for 30 min. The mixture was sealed in a 50 mL PTFE-lined stainless-steel autoclave and heated at 140 °C for 8 h. After collection by centrifugation, the final products were washed with anhydrous ethanol and distilled water three times and then dried at 80 °C for 4 h.

Synthesis of Mesoporous $BiVO_4$/Ag/AgCl Ternary HSMSs. In a typical procedure, 0.026 g of the as-prepared BiOCl microspheres and 0.5 g of PVP were dispersed into 15 mL of distilled water under stirring, to achieve mixture A. A 0.012 g portion of $NaVO_3$ was added into 10 mL of distilled water, to obtain solution B. Then solution B was added dropwise into mixture A after 2 h of continuous stirring, to obtain mixture C. A 0.02 M solution of $AgNO_3$ was added into 10 mL of distilled water, to get solution D. Solution D was added into mixture C dropwise, and then it was kept stirring for 2 h at room temperature. The collected products were washed with ethanol and distilled water three times before being dried at 80 °C for 4 h. Subsequently, the resulting mesoporous $BiVO_4$/AgCl binary HSMSs were obtained by calcination at 400 °C for 2 h in an air flow with a heating rate of 3.33 °C min^{-1}. Finally, the as-prepared $BiVO_4$/AgCl binary HSMSs were dispersed in water under stirring and then irradiated with visible light for 2 h to produce mesoporous $BiVO_4$/Ag/AgCl ternary HSMSs. For the purpose of comparison, pure $BiVO_4$ is also prepared by a simple solvothermal method.[22] In addition, the experimental procedure of other contrastive photocatalysts was in the Supporting Information.

Characterizations. Powder X-ray diffraction (XRD) measurements of the samples were performed with a Philips PW3040/60 X-ray diffractometer using Cu Kα radiation at a scanning rate of 0.06 deg s^{-1}. Scanning electron microscopy (SEM) was performed with a Hitachi S-4800 scanning electron microanalyzer with an accelerating voltage of 15 kV. Transmission electron microscopy (TEM) and high-resolution transmission electron microscopy (HRTEM) were conducted using a JEM-2100F field-emission TEM. For TEM measurements, samples were prepared by dispersing the products in ethanol and placing several drops of the suspension on holey carbon net supported on copper grids. Further evidence for the composition of the product was obtained from X-ray photoelectron spectroscopy (XPS), using a Kratos Axis ULTRA X-ray photoelectron spectrometer with Al Kα X-ray as the excitation source. UV−vis diffuse reflectance spectra (UV−vis DRS) of the as-prepared samples were recorded over the range 200−800 nm with the absorption mode using a Thermo Nicolet Evolution 500 UV−vis spectrophotometer equipped with an integrating sphere attachment. The absorption spectra were measured using a PerkinElmer Lambda 900 UV−vis spectrophotometer at room temperature. N_2 adsorption−desorption isotherms were obtained at 77 K on a Micrometrics ASAP 2020 surface area and porosity analyzer after the sample had been degassed in vacuum at 160 °C for 4 h. The total organic carbon (TOC) concentration was measured using a Liqui TOCII (ELEMENTAR Corporation) system.

Photocatalytic Test. The photocatalytic activities of the as-prepared samples were evaluated by the degradation of methyl orange (MO) and phenol under visible-light irradiation from a 500 W Xe lamp with a 420 nm cutoff filter. The reaction cell was placed in a sealed black box with the top open, and the distance between light source and solution surface is 20 cm. In a typical process, 5 or 10 mg of the as-prepared sample as photocatalyst was added into 20 mL of MO (concentration: 10 mg L^{-1}) or phenol solution (25 mg L^{-1}), respectively. After dispersion in an ultrasonic bath for 5 min, the solution was stirred for 1 h in the dark to reach adsorption equilibrium between the catalyst and the solution and then was exposed to visible-light irradiation. The samples were collected by centrifugation at given time intervals, and then the MO and phenol degradation concentrations were measured by UV−vis spectroscopy method.

3. RESULTS AND DISCUSSION

The crystallographic structure and phase purity of the as-obtained sample are first examined by XRD analysis. The XRD pattern of the as-prepared BiOCl microspheres (Figure S1a, in the Supporting Information) exhibits diffraction peaks of tetragonal-phase BiOCl with lattice constants of $a = b = 3.891$ Å, $c = 7.369$ Å (JCPDS card 06-0249). The XRD pattern of the as-prepared mesoporous $BiVO_4$/AgCl binary HSMSs (Figure 2) obtained by a facile solid-phase dual-ion-exchange process reveals only two sets of diffractions, one from the body-centered monoclinic phase of $BiVO_4$ ($a = 5.195$ Å, $b = 11.70$ Å, $c = 5.092$ Å, JCPDS card 14-0688), and the other from the cubic phase of AgCl ($a = b = c = 5.55$ Å, JCPDS card 31-1238). No impurity peaks are detectable, indicating the successful transformation of BiOCl to $BiVO_4$/AgCl heteronanostructures. After irradiation under visible-light for 2 h, besides the obvious $BiVO_4$ and AgCl diffraction peaks, a weak diffraction peak at 2θ of 38.1° denoted by a circle can be indexed to the (111) plane

DOI: 10.1021/acs.inorgchem.5b01303
Inorg. Chem. 2015, 54, 9033−9039

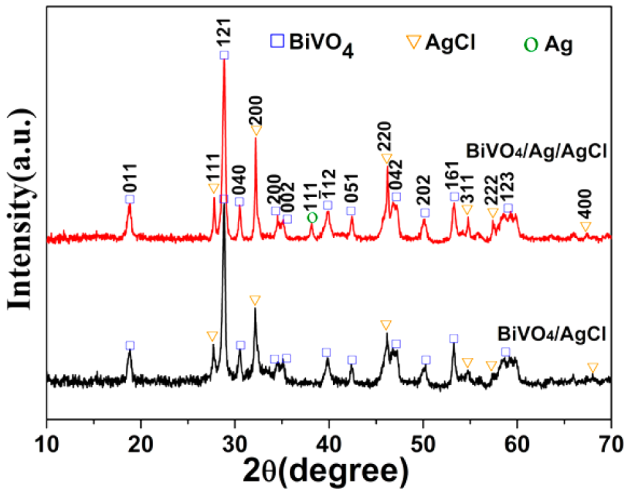

Figure 2. XRD patterns of the as-prepared mesoporous $BiVO_4$/AgCl binary and $BiVO_4$/Ag/AgCl ternary HSMSs.

of the cubic phase of Ag ($a = b = c = 4.09$ Å, JCPDS card 04-0783), implying that the Ag nanoparticles (NPs) are formed. The elemental composition and chemical states of the as-obtained mesoporous $BiVO_4$/Ag/AgCl ternary HSMSs were further investigated by XPS measurements, as displayed in Figure 3. The survey XPS spectrum (Figure 3a) confirms the existence of ingredient elements of Bi, V, O, Ag, and Cl in the as-prepared sample. Figure 3b shows the high-resolution spectrum of Ag 3d, which exhibits two obvious peaks, corresponding to Ag 3d5/2 and 3d3/2 binding energies, respectively. Specifically, the two Ag 3d peaks can be further resolved into four peaks by the XPS peak fitting program. The peaks at 367.8 and 373.8 eV originate from the Ag^+ ion, and the 368.2 and 374.2 eV peaks are metallic Ag^0 species, respectively.[31]

The morphology and microstructure of mesoporous $BiVO_4$/Ag/AgCl ternary HSMSs, as well as the as-prepared BiOCl microsphere precursor, are examined by SEM as shown in Figure 4. The low-magnification SEM image (Figure 4a) reveals uniform microspheres of the BiOCl precursor, with diameter of 1.4−1.6 μm, and the high-magnification image (Figure 4b) further indicates that the BiOCl hierarchical microsphere is assembled from irregular nanoflakes. The porous structure of the microspheres provides abundant active sites for the adsorption of VO_3^- and Ag^+ ions. SEM images of the $BiVO_4$/Ag/AgCl ternary HSMSs (Figure 4c,d) show that the

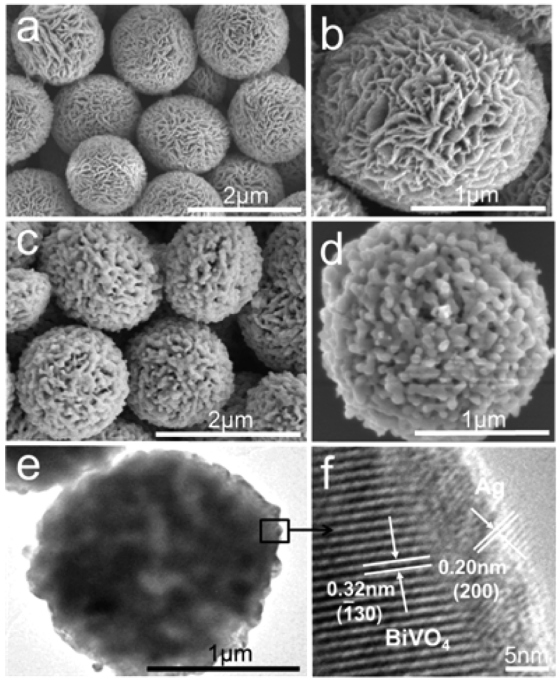

Figure 4. (a, b) SEM images of the as-prepared BiOCl microsoheres; (c, d) SEM, (e) TEM, and (f) HRTEM images of the as-obtained mesoporous $BiVO_4$/Ag/AgCl ternary HSMSs.

product well maintains the shape of the BiOCl precursor, but the surface structure of microspheres has been obviously modified. The original nanoflakes become thicker, and disordered wormhole-like pores are produced. This is a result of chemical transformation of BiOCl into porous $BiVO_4$/Ag/AgCl heteronanostructures. The geometrical structure of the mesoporous $BiVO_4$/Ag/AgCl ternary HSMSs is further elucidated by TEM observation (Figure 4e), which reveals the buildup of numerous irregular particles, in good agreement with the SEM results. Figure 4f shows a HRTEM image of the edge section of one $BiVO_4$/Ag/AgCl ternary HSMS, which clearly reveals the heterojunction region between the $BiVO_4$ and Ag metal. Due to the instability of AgCl under electron beam irradiation, only metallic Ag can be observed.[32] To reveal the spatial distribution of different elements in the hetero-nanostructure, elemental mapping is performed on one single ternary HSMS. As shown in Figure 5, the mapping results show uniform distribution of Bi, V, O, Ag, and Cl elements all over the whole HSMS, indicating that the exchange reaction occurs

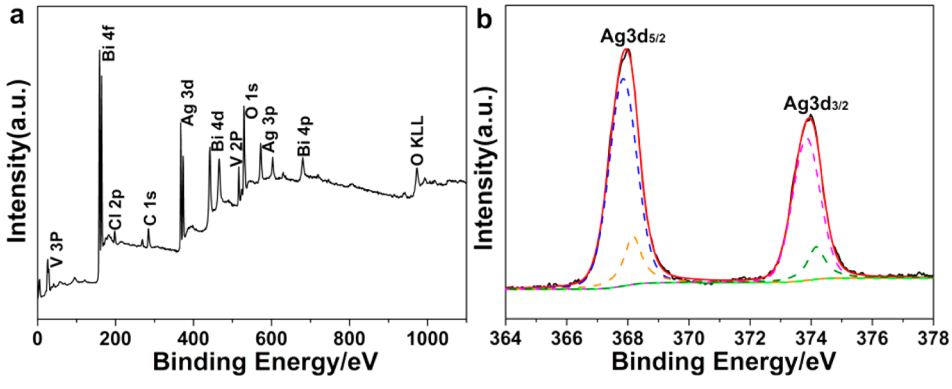

Figure 3. XPS spectra of the as-prepared $BiVO_4$/Ag/AgCl ternary HSMSs: (a) the survey XPS spectrum and (b) Ag 3d.

DOI: 10.1021/acs.inorgchem.5b01303
Inorg. Chem. 2015, 54, 9033−9039

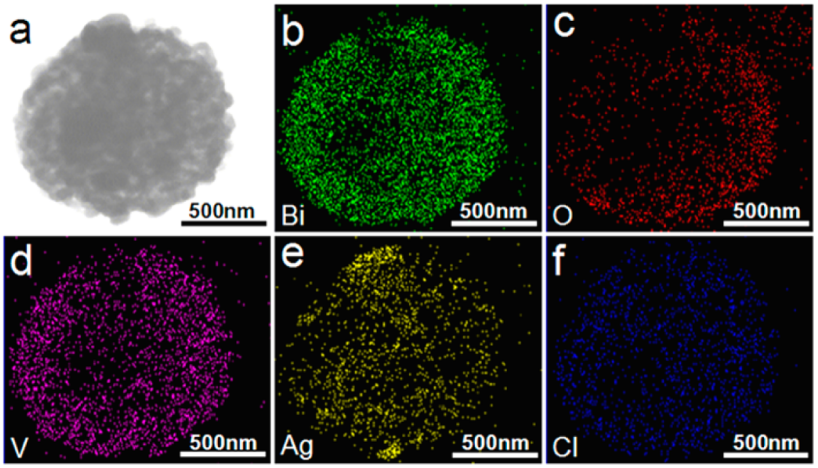

Figure 5. (a) STEM image of a representative $BiVO_4$/Ag/AgCl ternary HSMS and the corresponding elemental mappings of Bi (b), O (c), V (d), Ag (e), and Cl (f) elements.

uniformly in the whole BiOCl microsphere and results in the formation of mesoporous $BiVO_4$/Ag/AgCl ternary HSMSs.

Interestingly, it is found that the solid-phase dual-ion-exchange process can only take place in the presence of Ag^+ ions. If $AgNO_3$ is not added in the impregnation process, the product obtained after annealing remains as BiOCl and no other product such as $BiVO_4$ is detectable (XRD pattern, Figure S1b, in the Supporting Information). To further display the role of Ag^+ ions, the thermodynamic calculation of the reaction process was also investigated. For reaction 1, the Gibbs free energy $\Delta_r G_m(T)_{(1)} = \Delta_r H_m^\theta - T\Delta_r S_m^\theta = -43.29$ kJ mol^{-1}: this reaction can occur spontaneously. However, $\Delta_r G_m(T)_{(2)}$ is 7.60 kJ mol^{-1} for reaction 2; thus, this reaction cannot occur spontaneously. However, when reactions 1 and 2 are taken place simultaneously (BiOCl + VO_3^- + Ag^+ → $BiVO_4$ + AgCl), $\Delta_r G_m(T) = -43.29 + 7.60 = -35.69$ kJ mol^{-1} < 0. This suggests the formation of $BiVO_4$/AgCl HSMSs is achieved through a dual-ion-exchange process described by reactions 1 and 2, and the reaction of Ag^+ with Cl^- plays an indispensable role on the occurrence of reaction 2. The generation of pores can be attributed to the rapid kinetic and strain release in the ion-exchange reactions due to large lattice mismatch effect.[33] N_2 adsorption−desorption measurement is employed to characterize the porous structure of the as-prepared $BiVO_4$/Ag/AgCl ternary HSMSs, as shown in Figure 6. N_2 adsorption−desorption isotherm of the sample $BiVO_4$/Ag/AgCl HSMSs can be classified as a type IV isotherm with a distinct hysteresis loop, indicating the existence of abundant mesopores in the product.[34,35] The Barrett−Joyner−Halenda (BJH) pore-size distribution curve (inset in Figure 6) shows that the average size of the pores is mainly centered around 3.5 nm. These mesoporous channels are anticipated to facilitate the diffusion of pollutants into the heterostructured particles, which may greatly improve the photocatalytic activity of the hybrid semiconductor system. The UV−vis DRS data of the as-prepared pure $BiVO_4$, $BiVO_4$/Ag, and $BiVO_4$/Ag/AgCl ternary HSMSs are presented in Figure S2 (in the Supporting Information). Compared with the pure $BiVO_4$, the sample $BiVO_4$/Ag heterostructures exhibit a much stronger response in the visible region than pure $BiVO_4$, which should be attributed to the surface plasmon resonance (SPR) of the Ag NPs on the surfaces of $BiVO_4$/Ag.[36] In contrast with $BiVO_4$ and $BiVO_4$/Ag, $BiVO_4$/Ag/AgCl ternary HSMSs photocatalyst obviously

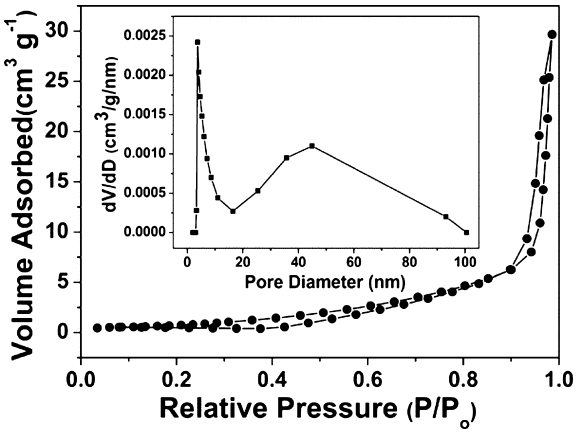

Figure 6. N_2 adsorption−desorption isotherm and pore-size distribution curve (inset) of the as-obtained mesoporous $BiVO_4$/Ag/AgCl ternary HSMSs.

exhibits broad absorption in the 500−800 nm region, indicating that the sample is beneficial for improving photocatalyic activity.

We have investigated the photocatalytic properties of the as-prepared mesoporous $BiVO_4$/Ag/AgCl ternary HSMSs. Figure 7a shows the photodegradation of an organic dye MO by pure $BiVO_4$, $BiVO_4$/Ag, mechanical mixture of $BiVO_4$ and AgCl, $BiVO_4$/AgCl binary HSMSs, and $BiVO_4$/Ag/AgCl ternary HSMSs under visible-light irradiation, where C is the concentration of MO after light irradiation for a certain period of time, and C_0 is the concentration of MO at adsorption/desorption equilibrium in dark. After irradiation for 60 min, nearly 95.4% of MO is degraded by sample $BiVO_4$/Ag/AgCl ternary HSMSs, while the other samples, including pure $BiVO_4$, $BiVO_4$/Ag, mechanical mixture of $BiVO_4$ and AgCl, and $BiVO_4$/AgCl binary HSMSs, exhibit lower degradation rates of about 13.5%, 22.9%, 46.4%, and 81.6%, respectively. Compared with the pure $BiVO_4$, the $BiVO_4$/Ag catalyst shows limited enhancement on the photodegradation of MO. Due to the SPR effect, the photoexcited electrons produced on the Ag NPs in the $BiVO_4$/Ag interface may be transferred to the surface of $BiVO_4$, which enhances the electron−hole pair separation of $BiVO_4$. The photocatalytic activity of a mechanical mixture of $BiVO_4$ and AgCl is enhanced after irradiation for several

DOI: 10.1021/acs.inorgchem.5b01303
Inorg. Chem. 2015, 54, 9033−9039

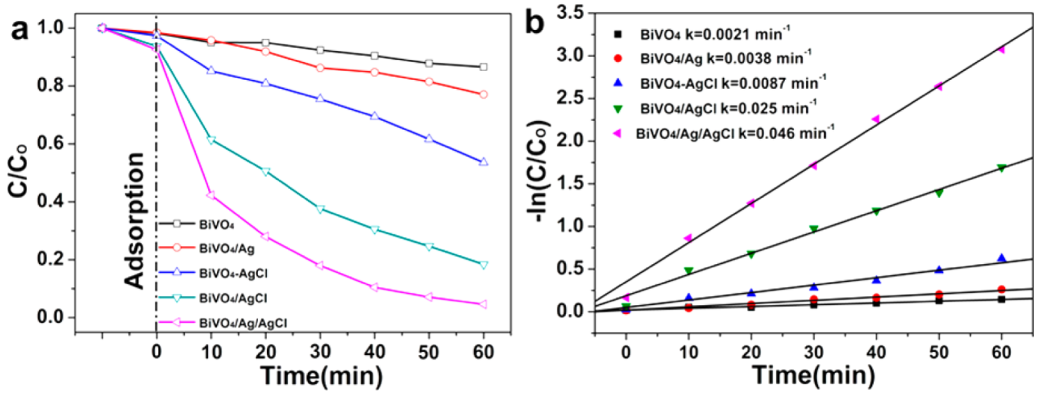

Figure 7. (a) Photodegradation of MO in the presence of different samples under visible-light irradiation. (b) Photodegradation kinetics of MO aqueous solutions over various photocatalysts.

minutes, which may be attributed to the production of Ag NPs on the surface of AgCl. Thus, the coexistence of Ag and AgCl on the surface of $BiVO_4$ is responsible for the high photocatalytic activity when irradiated by visible light.[36] It can be seen that the as-prepared $BiVO_4$/AgCl binary HSMSs exhibits higher photocatalytic reduction ability than pure $BiVO_4$, and the sample of $BiVO_4$/Ag/AgCl ternary HSMSs displays the highest photocatalytic activity among all the samples. Generally, when the pollutant is within the millimolar concentration range, the influence of the initial concentration of most organic compounds on the photodegradation rate is usually described by pseudo-first-order kinetics in terms of the Langmuir−Hinshelwood model eq 3.[37]

$$\ln C_t = -kt + \ln C_0 \quad (3)$$

Here C_0 is the initial dye concentration, C_t is the dye concentration in solution at times t, and k is the apparent first-order rate constant.[38] The kinetic plots of the different samples are displayed in Figure 7b. It can be seen that the rate constant of the photodegradation of MO using sample $BiVO_4$/Ag/AgCl ternary HSMSs as photocatalyst is 0.046 min^{-1}, which is much higher than that of other samples.

A TOC test was performed to further investigate the activity of $BiVO_4$/Ag/AgCl ternary HSMSs (Figure S3).[39,40] The result shows that the mineralization yield of $BiVO_4$/Ag/AgCl ternary HSMSs for the degradation of MO reaches a value of 48.0% after 60 min of irradiation. The rate of TOC reduction of $BiVO_4$/Ag/AgCl ternary HSMSs is slower than that of the degradation of dye, which is nearly 100% discoloration of MO in 60 min. This result indicates that the MO decolorization is partially decomposed into H_2O and CO_2. We have further studied the stability and reusability of the as-prepared ternay HSMSs photocatalyst by collecting and reusing the same photocatalyst for 10 cycles, and the results are shown in Figure S4 (in the Supporting Information). Only insignificant loss in photocatalytic activity is observed, which might be partly caused by incomplete collection of the photocatalyst during each cycle. The XRD pattern (Figure S5, in the Supporting Information) of the as-prepared ternary HSMSs after 10 cycles indicates almost no deterioration in the crystal structure. Additionally, the mesoporous $BiVO_4$/Ag/AgCl ternary HSMSs also exhibits high photocatalytic efficiency for the degradation of refractory organic pollutant of phenol (Figure S6a,b, in the Supporting Information). After irradiation for 180 min, nearly 43.0% and 22.1% (Figure S6c) of phenol is degraded by sample $BiVO_4$/Ag/AgCl ternary HSMSs and $BiVO_4$/AgCl binary HSMSs.

In order to identify the major active species in the photodegradation process, radical-trapping measurements are also performed, as displayed in Figure 8. The photodegradation

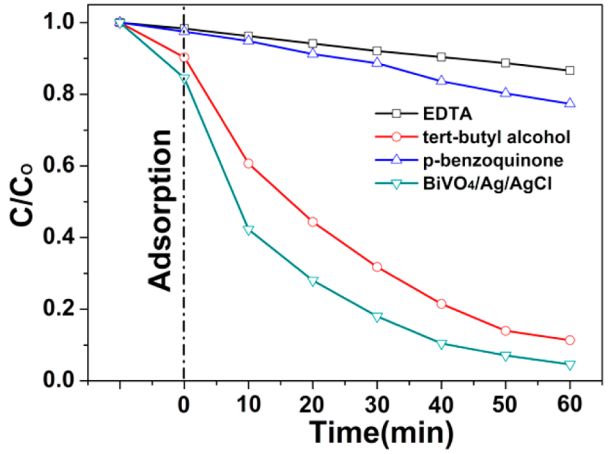

Figure 8. Plots of active species trapped in the system for the photodegradation of MO using the as-obtained $BiVO_4$/Ag/AgCl ternary HSMSs as photocatalyst.

of MO is slightly inhibited by the addition of 1 mM tert-butanol (a hydroxyl radical scavenger) under visible-light irradiation for 60 min,[41] indicating that the $^{\bullet}OH$ radicals are the minor active oxidizing species in the photoreaction process, while the MO concentration remains almost unchanged with the use of 1 mM of disodium ethylenediaminetetraacetate (Na_2-EDTA, a hole scavenger) and benzoquinone (a superoxide anion radical scavenger, $O_2^{\bullet-}$). Therefore, the photogenerated holes and $O_2^{\bullet-}$ are the dominant reactive species contributing to the oxidative degradation of MO. On the basis of the bandgap structures of $BiVO_4$ and AgCl and the effects of scavengers, a possible plasmonic Z-scheme mechanism is proposed and illustrated in Scheme 1. The energy bandgap of $BiVO_4$ is 2.40 eV, and the conduction band (CB) and valence band (VB) energy levels of $BiVO_4$ are about 0.33 and 2.73 eV (vs standard hydrogen electrode (SHE)),[42] respectively. The VB holes of $BiVO_4$ own a large oxidation power for the oxidation of organic pollutants owing to the high potential.[43] The CB and VB energy levels of AgCl are about −0.06 and 3.20 eV (vs SHE),[44] respectively, and hence AgCl cannot be excited

DOI: 10.1021/acs.inorgchem.5b01303
Inorg. Chem. 2015, 54, 9033−9039

Scheme 1. Schematic Diagram Showing the Possible Charge Transfer Process in the $BiVO_4$/Ag/AgCl Ternry Heterostructure

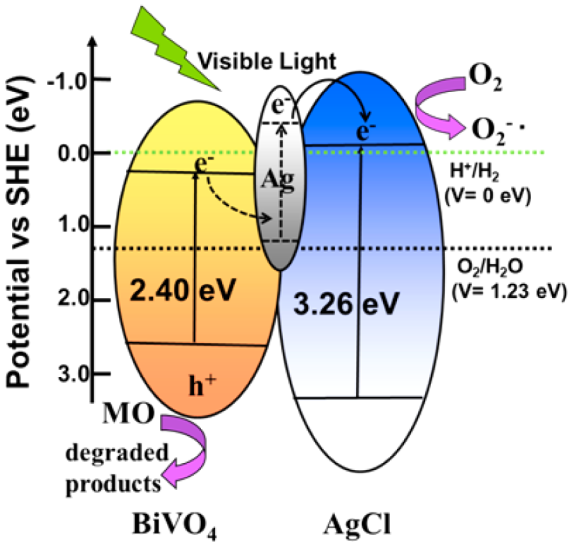

under visible-light irradiation due to its large bandgap. Considering the $O_2^{\bullet-}$ is one of the main active species, electrons in the CB of $BiVO_4$ could not reduce O_2 to generate $O_2^{\bullet-}$ active species because the CB potential of $BiVO_4$ (0.33 eV vs SHE) is more positive than the reduction potential of oxygen E^0 ($O_2/O_2^{\bullet-}$) (−0.046 eV vs SHE).[42] The active photoelectrons on the Ag NPs may be injected into the CB of AgCl and react with the ubiquitous molecular oxygen to form the superoxide radical $O_2^{\bullet-}$, which can contribute to the decomposition of MO.[43,45−47] Simultaneously, the photogenerated electrons in the CB of $BiVO_4$ transfer to the low-energy states in Ag NPs and are ready to be excited to higher states as hot electrons by the SPR effect,[48] while the photoexcited holes remain in the VB of $BiVO_4$ to directly oxidize the dye molecule.[49] The spontaneous transfer of electrons and holes in the $BiVO_4$/Ag/AgCl ternary heterostructure increases both the yield and lifetime of charge carriers by effectively separating them and reducing the chance for recombination, and thus demonstrates the highest photocatalytic activity.[50]

4. CONCLUSIONS

In summary, we have demonstrated a simple and novel solid-phase dual-ion-exchange strategy together with subsequent visible-light induced reduction for the synthesis of uniform mesoporous $BiVO_4$/Ag/AgCl ternary HSMSs. Hierarchical BiOCl microspheres synthesized by a hydrothermal method are used as the precursor. Benefiting from the unique structural features, the as-prepared $BiVO_4$/Ag/AgCl ternary heteronanostructures exhibit excellent photocatalytic activity and favorable recyclability for the degradation of organic dye under visible-light irradiation. The photocatalytic mechanism is investigated. We believe that this new synthesis strategy is not restricted to the specific materials discussed in this work and can be extended to the preparation of a wide range of porous microstructures for various applications.

■ ASSOCIATED CONTENT

Ⓢ Supporting Information

The Supporting Information is available free of charge on the ACS Publications website at DOI: 10.1021/acs.inorgchem.5b01303.

Synthesis of $BiVO_4$/AgCl and Figures S1−S6 (PDF)

■ AUTHOR INFORMATION

Corresponding Authors

*E-mail: yizhong@zjnu.cn.
*E-mail: jqning2015@sinano.ac.cn.
*E-mail: yonghu@zjnu.edu.cn.

Author Contributions

R.Q. and M.M. contributed equally to this work.

Notes

The authors declare no competing financial interest.

■ ACKNOWLEDGMENTS

We acknowledge the financial support from the Natural Science Foundation of China (21171146, 21371152) and the Zhejiang Provincial Natural Science Foundation of China (LR14B010001). The authors thank Dr. X. W. Lou (Nanyang Technological University) for enlightening discussions.

■ REFERENCES

(1) Zheng, Y. H.; Chen, C. Q.; Zhan, Y. Y.; Lin, X. Y.; Zheng, Q.; Wei, K. M.; Zhu, J. F. *J. Phys. Chem. C* **2008**, *112*, 10773−10777.
(2) Yang, W. L.; Zhang, L.; Hu, Y.; Zhong, Y. J.; Wu, H. B.; Lou, X. W. *Angew. Chem., Int. Ed.* **2012**, *51*, 11501−11504.
(3) Kang, J.; Kuang, Q.; Xie, Z. X.; Zheng, L. S. *J. Phys. Chem. C* **2011**, *115*, 7874−7879.
(4) Yu, J. G.; Dai, G. P.; Huang, B. B. *J. Phys. Chem. C* **2009**, *113*, 16394−16401.
(5) Morimoto, T.; Suzuki, K.; Torikoshi, M.; Kawahara, T.; Tada, H. *Chem. Commun.* **2007**, 4291−4293.
(6) Li, J. J.; Yang, W. L.; Ning, J. Q.; Zhong, Y. J.; Hu, Y. *Nanoscale* **2013**, *6*, 5612−5615.
(7) Subramanian, V.; Wolf, E. E.; Kamat, P. V. *J. Am. Chem. Soc.* **2004**, *126*, 4943−4950.
(8) Niu, H. H.; Zhang, S. W.; Wang, R. B.; Guo, Z. Q.; Shang, X.; Gan, W.; Qin, S. X.; Wan, L.; Xu, J. Z. *J. Phys. Chem. C* **2014**, *118*, 3504−3513.
(9) Liang, J.; Du, X.; Gibson, C.; Du, X. W.; Qiao, S. Z. *Adv. Mater.* **2013**, *25*, 6226−6231.
(10) Zhang, X. S.; Zhu, F. Y.; Han, M. D.; Sun, X. M.; Peng, X. H.; Zhang, H. X. *Langmuir* **2013**, *29*, 10769−10775.
(11) Wang, H. K.; Xi, L. J.; Tucek, J.; Zhan, Y. W.; Hung, T. F.; Kershaw, S. V.; Zboril, R.; Chung, C. Y.; Rogach, A. L. *Nanoscale* **2013**, *5*, 9101−9109.
(12) Huang, X. Q.; Zhang, H. H.; Guo, C. Y.; Zhou, Z. Y.; Zheng, N. F. *Angew. Chem.* **2009**, *121*, 4902−4906.
(13) Puigmarti-Luis, J.; Schaffhauser, D.; Burg, B. R.; Dittrich, P. S. *Adv. Mater.* **2010**, *22*, 2255−2259.
(14) Zhang, X. Y.; Lu, W.; Dai, J. Y.; Bourgeois, L.; Hao, N.; Wang, H. T.; Zhao, D. Y.; Webley, P. A. *Angew. Chem., Int. Ed.* **2010**, *49*, 10101−10105.
(15) Li, W. Y.; Li, G.; Sun, J. Q.; Zou, R. J.; Xu, K. B.; Sun, Y. G.; Chen, Z. G.; Yang, J. M.; Hu, J. Q. *Nanoscale* **2013**, *5*, 2901−2908.
(16) Zhang, H.; Wang, H.; Xu, Y.; Zhuo, S. F.; Yu, Y. F.; Zhang, B. *Angew. Chem., Int. Ed.* **2012**, *51*, 1459−1463.
(17) Chen, L.; Zhang, Q.; Huang, R.; Yin, S. F.; Luo, S. L.; Au, C. T. *Dalton Trans.* **2012**, *41*, 9513−9518.
(18) Zhou, H.; Ding, L.; Fan, T. X.; Ding, J.; Zhang, D.; Guo, Q. X. *Appl. Catal., B* **2014**, *147*, 221−228.

DOI: 10.1021/acs.inorgchem.5b01303
Inorg. Chem. 2015, 54, 9033−9039

(19) Xiao, X.; Liu, C.; Hu, R. P.; Zuo, X. X.; Nan, J. M.; Li, L. S.; Wang, L. S. *J. Mater. Chem.* **2012**, *22*, 22840−22843.
(20) He, Z. Q.; Shi, Y. Q.; Gao, C.; Wen, L. N.; Chen, J. M.; Song, S. *J. Phys. Chem. C* **2014**, *118*, 389−398.
(21) Jin, R. X.; Yang, Y.; Xing, Y.; Chen, L.; Song, S. Y.; Jin, R. C. *ACS Nano* **2014**, *8*, 3664.
(22) Gao, X. H.; Wu, H. B.; Zheng, L. X.; Zhong, Y. J.; Hu, Y.; Lou, X. W. *Angew. Chem., Int. Ed.* **2014**, *53*, 5917−5921.
(23) Rao, P. M.; Cai, L. L.; Liu, C.; Cho, I. S.; Lee, C. H.; Weisse, J. M.; Yang, P. D.; Zheng, X. L. *Nano Lett.* **2014**, *14*, 1099−1105.
(24) Li, C. J.; Zhang, P.; Lv, R.; Lu, J. W.; Wang, T.; Wang, S. P.; Wang, H. F.; Gong, J. L. *Small* **2013**, *9*, 3951−3956.
(25) Chatchai, P.; Kishioka, S.-Y.; Murakami, Y.; Nosaka, A. Y.; Nosaka, Y. *Electrochim. Acta* **2010**, *55*, 592−596.
(26) Agrawal, M.; Gupta, S.; Pich, A.; Zafeiropoulos, N. E.; Stamm, M. *Chem. Mater.* **2009**, *21*, 5343−5348.
(27) Lv, K.; Li, J.; Qing, X. X.; Li, W. Z.; Chen, Q. Y. *J. Hazard. Mater.* **2011**, *189*, 329−335.
(28) Wan, W. Z.; Huang, X. W.; Wu, S.; Zhou, Y. X.; Wang, L. J.; Shi, H. L.; Liang, Y. J.; Zou, B. *Appl. Catal., B* **2013**, *134*, 293−301.
(29) Wetchakun, N.; Chaiwichain, S.; Inceesungvorn, B.; Pingmuang, K.; Phanichphant, S.; Minett, A. I.; Chen, J. *ACS Appl. Mater. Interfaces* **2012**, *4*, 3718−3723.
(30) Zhou, L.; Zhao, D. Y.; Lou, X. W. *Angew. Chem., Int. Ed.* **2012**, *51*, 239−241.
(31) Li, H. Y.; Sun, Y. J.; Bin, C.; Gan, S. Y.; Han, D. X.; Li, N.; Wu, T. S. *Appl. Catal., B* **2015**, *170−171*, 206−214.
(32) Longo, E.; Cavalcante, L. S.; Volanti, D. P.; Gouveia, A. F.; Longo, V. M.; Varela, J. A.; Orlandi, M. O.; Andrés, J. *Sci. Rep.* **2013**, *3*, 1676.
(33) Wu, X.; Yu, Y. F.; Liu, Y.; Xu, Y.; Liu, C. B.; Zhang, B. *Angew. Chem., Int. Ed.* **2012**, *51*, 3211−3215.
(34) Xingfu, Z.; Zhaolin, H.; Yiqun, F.; Su, C.; Weiping, D.; Nanping, X. *J. Phys. Chem. C* **2008**, *112*, 11722−11728.
(35) Kruk, M.; Jaroniec, M. *Chem. Mater.* **2001**, *13*, 3169−3183.
(36) Ma, B. W.; Guo, J. F.; Dai, W. L.; Fan, K. N. *Appl. Catal., B* **2012**, *123*, 193−199.
(37) Geng, Y. L.; Zhang, P.; Kuang, S. P. *RSC Adv.* **2014**, *4*, 46054−46059.
(38) Li, J. J.; Xie, Y. L.; Zhong, Y. J.; Hu, Y. *J. Mater. Chem. A* **2015**, *3*, 5474−5481.
(39) Wang, D. J.; Guo, L.; Zhen, Y. Z.; Yue, L. L.; Xue, G. L.; Fu, F. *J. Mater. Chem. A* **2014**, *2*, 11716−11727.
(40) Hao, Z. Q.; Xu, L. L.; Wei, B.; Fan, L. L.; Liu, Y.; Zhang, M. Y.; Gao, H. *RSC Adv.* **2015**, *5*, 12346−12353.
(41) Tang, J. T.; Liu, Y. H.; Li, H. Z.; Tan, Z.; Li, D. T. *Chem. Commun.* **2013**, *49*, 5498−5500.
(42) Long, M. C.; Cai, W. M.; Cai, J.; Zhou, B. X.; Chai, X. Y.; Wu, Y. H. *J. Phys. Chem. B* **2006**, *110*, 20211−20216.
(43) Yao, X. X.; Liu, X. H. *J. Hazard. Mater.* **2014**, *280*, 260−268.
(44) Wang, X. F.; Li, S. F.; Ma, Y. Q.; Yu, H. G.; Yu, J. G. *J. Phys. Chem. C* **2011**, *115*, 14648−14655.
(45) Wang, P.; Huang, B. B.; Qin, X. Y.; Zhang, X. Y.; Dai, Y.; Wei, J. Y.; Whangbo, M. H. *Angew. Chem., Int. Ed.* **2008**, *47*, 7931−7933.
(46) Schűrch, D.; Currao, A.; Sarkar, S.; Hodes, G.; Calzaferri, G. *J. Phys. Chem. B* **2002**, *106*, 12764−12755.
(47) Hou, J. G.; Yang, C.; Wang, Z.; Ji, Q. H.; Li, Y. T.; Huang, G. C.; Jiao, S. Q.; Zhu, H. M. *Appl. Catal., B* **2013**, *142−143*, 579−589.
(48) Li, Z.; Ezhilarasu, G.; Chatzakis, I.; Dhall, R.; Chen, C. C.; Cronin, S. B. *Nano Lett.* **2015**, *15*, 3977−3982.
(49) Hou, J. G.; Wang, Z.; Yang, C.; Zhou, W. L.; Jiao, S. Q.; Zhu, H. M. *J. Phys. Chem. C* **2013**, *117*, 5132−5141.
(50) Guo, J. F.; Ma, B. W.; Yin, A. Y.; Fan, K. N.; Dai, W. L. *J. Hazard. Mater.* **2012**, *211*, 77−82.

DOI: 10.1021/acs.inorgchem.5b01303
Inorg. Chem. 2015, 54, 9033−9039